



Article

Cite this article: Prior-Jones MR et al. (2021). Cryoegg: development and field trials of a wireless subglacial probe for deep, fast-moving ice. *Journal of Glaciology* 1–14. <https://doi.org/10.1017/jog.2021.16>

Received: 12 June 2020
Revised: 27 January 2021
Accepted: 28 January 2021

Keywords:

Glacier hydrology; glaciological instruments and methods; subglacial processes

Author for correspondence:

Michael Prior-Jones,
E-mail: prior-jonesm@cardiff.ac.uk;
Elizabeth A. Bagshaw,
E-mail: bagshawe@cardiff.ac.uk

Cryoegg: development and field trials of a wireless subglacial probe for deep, fast-moving ice

Michael R. Prior-Jones¹ , Elizabeth A. Bagshaw¹ , Jonathan Lees², Lindsay Clare³, Stephen Burrow³, Mauro A. Werder^{4,5} , Nanna B. Karlsson⁶ , Dorthe Dahl-Jensen^{7,8} , Thomas R. Chudley⁹ , Poul Christoffersen⁹ , Jemma L. Wadham¹⁰, Samuel H. Doyle¹¹ and Bryn Hubbard¹¹

¹School of Earth and Environmental Sciences, Cardiff University, Cardiff, UK; ²School of Engineering, Cardiff University, Cardiff, UK; ³Department of Aerospace Engineering, University of Bristol, Bristol, UK; ⁴Laboratory of Hydraulics, Hydrology and Glaciology (VAW), ETH Zürich, Zürich, Switzerland; ⁵Swiss Federal Institute for Forest, Snow and Landscape Research (WSL), Birmensdorf, Switzerland; ⁶Geological Survey of Denmark and Greenland, Copenhagen, Denmark; ⁷Niels Bohr Institute, University of Copenhagen, Copenhagen, Denmark; ⁸Center for Earth Observation Science, University of Manitoba, Winnipeg, Canada; ⁹Scott Polar Research Institute, University of Cambridge, Cambridge, UK; ¹⁰School of Geographical Sciences, University of Bristol, Bristol, UK and ¹¹Department of Geography and Earth Sciences, Aberystwyth University, Aberystwyth, UK

Abstract

Subglacial hydrological systems require innovative technological solutions to access and observe. Wireless sensor platforms can be used to collect and return data, but their performance in deep and fast-moving ice requires quantification. We report experimental results from Cryoegg: a spherical probe that can be deployed into a borehole or moulin and transit through the subglacial hydrological system. The probe measures temperature, pressure and electrical conductivity in situ and returns all data wirelessly via a radio link. We demonstrate Cryoegg's utility in studying englacial channels and moulins, including in situ salt dilution gauging. Cryoegg uses VHF radio to transmit data to a surface receiving array. We demonstrate transmission through up to 1.3 km of cold ice – a significant improvement on the previous design. The wireless transmission uses Wireless M-Bus on 169 MHz; we present a simple radio link budget model for its performance in cold ice and experimentally confirm its validity. Cryoegg has also been tested successfully in temperate ice. The battery capacity should allow measurements to be made every 2 h for more than a year. Future iterations of the radio system will enable Cryoegg to transmit data through up to 2.5 km of ice.

Introduction

The presence and behaviour of liquid water in the subglacial environment govern the response of ice to climate warming. Meltwater generated on the surface makes its way to the bed via networks of moulins, cracks and crevasses (Chu, 2014; Flowers, 2018). Once at the bed, it flows to the ice margins either through a subglacial drainage network consisting of inefficient linked cavities (Iken and Bindshadler, 1986; Walder, 1986; Kamb, 1987), efficient channels carved into rock, ice or the sediment below (Röthlisberger, 1972; Nye, 1976; Clarke, 1987; Ng, 2000), or a combination of both (Hoffman and others, 2016). The configuration of the drainage network determines the subglacial water pressure and how much of the ice-bed interface is in contact with liquid water. Contact promotes sliding (Kamb, 1970; Iken, 1981; Schoof, 2010), which in turn can cause ice to accelerate downstream. In recent years, the relationship between meltwater supply and ice acceleration has been reevaluated in light of observations from the margins of the Greenland Ice Sheet that demonstrate a seasonal evolution of subglacial drainage systems (Chandler and others, 2013; Tedstone and others, 2015) commonly observed in Alpine systems (Nienow and others, 2005). Early in the melt season, an increased flux of meltwater is routed to the bed and the low capacity, inefficiently linked cavity system is forced to expand, forming efficient channels that can transport substantial volumes of water. This reduces the area of the bed in contact with water, and potentially regulates the flow of ice (Sole and others, 2011; Tedstone and others, 2015; Nienow and others, 2017; Flowers, 2018). The defining feature of these different drainage configurations is the water pressure: channelised systems operate at lower pressure than linked cavities, thus measurement of the subglacial water pressure can be used to determine the likely structure of the drainage system, and hence the acceleration response of the ice to increased surface melt inputs.

In addition to water pressure, other parameters may provide clues as to the structure of the drainage system, but distinction between drainage system types is challenging. Temperature can be used to assess whether the bed is at the pressure melting point, and the residence time of water in the system can be used, in conjunction with pressure, to assess how efficiently the meltwater transits the system. Long residence times are common in linked cavity systems, which results in prolonged contact between meltwater and subglacial sediment (Tranter and others, 2002). This promotes chemical weathering and changes the composition of the meltwater, so meltwater

© The Author(s), 2021. Published by Cambridge University Press. This is an Open Access article, distributed under the terms of the Creative Commons Attribution licence (<http://creativecommons.org/licenses/by/4.0/>), which permits unrestricted re-use, distribution, and reproduction in any medium, provided the original work is properly cited.

cambridge.org/jog

chemistry is a good indicator of drainage system structure. Chemical composition is challenging to assess in situ, but a measurement of the total dissolved solids can be easily obtained via a measurement of electrical conductivity (Hubbard and others, 1995).

These three parameters (pressure (P), temperature (T) and electrical conductivity (EC)) are relatively easy to measure via electronic sensors and can thus be combined to provide information on subglacial drainage that could not be detected from the surface. Measuring these parameters subglacially is, however, extremely challenging, particularly beneath thick, fast-flowing ice. Yet it is these fast-flowing sectors that govern the response of large ice masses to climate warming, since they transfer significant volumes of ice to the ocean (Pritchard and others, 2009; van den Broeke and others, 2016). Drilling boreholes through a glacier to access subglacial hydrological channels is logistically demanding and disturbs the system that is under study. Once boreholes are drilled, implanting cabled sensors is possible, but ice motion causes cables to flex and eventually break (Iken and others, 1993; Doyle and others, 2018). In fast-flowing ice, data capture is thus limited to days or weeks. An alternative method is therefore required that can capture these relatively simple electrical measurements and return them to the surface without requiring a physical connection. A wireless radio frequency (RF) system is ideal and there is a long history of the use of RF propagation through ice (see Plewes and Hubbard, 2001 for a review).

Here, we present trials of Cryoegg, a wireless sensor platform for use in deep ice. The use of a radio link for subglacial telemetry has been proven by the work of the Glacsweb programme (Martinez and others, 2004; Hart and others, 2019) and the WiSe project (Smeets and others, 2012). Previous work (Bagshaw and others, 2014) showed that a ‘Cryoegg’ concept was feasible, namely a spherical sensor platform containing all sensor, radio and datalogger components that could fit in a standard borehole and travel through subglacial meltwater pathways: the electronics could be made sufficiently compact, and that the radio link worked through up to 500 m of ice. However, the radio link design chosen proved unsuitable for performance in very deep ice, so design improvements were required. In this paper, we describe the redesign of Cryoegg to give enhanced radio link performance and show the outcomes of field trials at sites in Greenland and the Swiss Alps.

In order to measure subglacial hydrological properties in deep polar ice, the enhanced Cryoegg had to meet or exceed the following engineering constraints:

- An outer diameter of 120 mm or less, to fit into a standard ice core borehole
- A radio link capable of reaching the surface through 2500 m of ice, the mean bed depth in central Greenland (Morlighem and others, 2017)
- Survive and measure water pressure of up to 25 MPa (250 bar, equivalent to a water column of 2500 m)
- Measure temperature, typically in the range from -30 to 0°C
- Measure EC, typically in the range from 0.002 to 25 mS m^{-1} ($2\text{--}250\text{ }\mu\text{S cm}^{-1}$)
- A battery life capable of sustaining one measurement every 12 h for a period of 1 year

Radio link design

The success of the instrument depends principally on the performance of the radio link. The 2012 design (Bagshaw and others, 2014) used a simple frequency shift keying transmitter operating on 151 MHz and demonstrated a maximum range of 500 m in wet ice. To achieve a greater range, we investigated alternative frequencies and transmission schemes. The power of a radio wave propagating in ‘free space’ (e.g. in air or vacuum) reduces

Table 1. Values of free space path loss in dB for several frequencies used by previous subglacial wireless transmission systems, the industrial standard LoRaWAN and the redesign of Cryoegg (see Results section). The shaded column indicates the values that apply to the radio link design described in this paper.

System	WiSe ^a	eTracer ^b , Cryoegg (2012) ^b , Glacsweb (2012–present) ^c	Glacsweb (2004–2006) ^d	LoRaWAN ^e	Cryoegg (2019)
Frequency (MHz)	30	150	433	868	169
Distance (m)					
100	42.0	56.0	65.2	71.2	57.0
500	56.0	70.0	79.2	85.2	71.0
1000	62.0	76.0	85.2	91.2	77.0
1500	65.5	79.5	88.7	94.7	80.5
2000	68.0	82.0	91.2	97.2	83.0
2500	70.0	83.9	93.1	99.2	85.0

^aSmeets and others (2012); ^bBagshaw and others (2014); ^cHart and others (2019); ^dMartinez and others (2004); ^e<https://lora-alliance.org/about-lorawan/>.

according to an inverse square law with distance – known as ‘geometric attenuation’. When the propagating wave reaches a receiving antenna, the ability of that antenna to extract power from the incoming wave is the ‘effective aperture’, and this depends upon the wavelength of the incoming wave. Antenna performance is more usually characterised using the antenna gain, which is the ratio of the antenna’s effective aperture in the direction of the main beam to the effective aperture of an ‘ideal’ isotropic antenna that receives signals equally well in all directions.

These effects are collectively described by the free space path loss (FSPL) equation, sometimes known as the Friis transmission equation, which describes how a radio link performs in free space. The equation assumes that the antennas are optimally pointed at one another and that their polarisations match, otherwise there are further losses associated with pointing error and polarisation mismatch. The original paper (Friis, 1946) presents the equation in terms of effective aperture, and in linear units. The more commonly used version quoted here is expressed in terms of antenna gain and uses decibel units.

Equation (1), adapted from Griffiths (1987, p. 12), is the FSPL equation in decibel units:

$$P_{\text{rx}} = P_{\text{tx}} + G_{\text{tx}} + G_{\text{rx}} - 20 \log_{10} \left(\frac{4\pi d}{\lambda} \right), \quad (1)$$

- P_{rx} is the power at the receiver, in dBW (dB relative to 1 watt)
- P_{tx} is the power transmitted by the transmitter, in dBW
- G_{tx} is the gain of the transmitting antenna, in dBi (dB relative to the performance of an isotropic antenna)
- G_{rx} is the gain of the receiving antenna, in dBi
- d is the distance between the transmitting and receiving antennas in metres
- λ is the wavelength of the transmission.

The last term of Eqn (1) is known as the ‘free space path loss’ (FSPL) and combines the geometric attenuation due to distance with the apparent wavelength-related attenuation caused by the effective aperture of the antennas. Consequently, the FSPL equation gives us the rule of thumb that lower frequencies (longer wavelengths) appear to propagate further than higher frequencies. FSPL over 2500 m ranges from 70 dB at 30 MHz to 99 dB at 868 MHz (Table 1), depending on frequency.

FSPL applies to all radio links regardless of the propagating medium. However, where the medium is lossy, the signal is

Table 2. Attenuation length and corresponding attenuation coefficient from 100 to 5000 m

Attenuation length (L_α), metres	Attenuation coefficient (α), dB km ⁻¹
100	86.9
200	43.4
300	29.0
400	21.7
500	17.4
600	14.5
700	12.4
800	10.9
900	9.7
1000	8.7
1500	5.8
2000	4.3
5000	1.7

further attenuated by the interaction between the wave and the medium. Ice is one such lossy medium. While simple models can predict RF attenuation in pure ice, in reality, glacier ice is heterogeneous, varying in temperature, pore water and impurity content and it contains cracks, water pockets and debris. Ultra-high frequencies (300 MHz–3 GHz) have been effective for transmission through deep, cold and uniform ice (Lewis and others, 2015), but any presence of water in this matrix quickly reduces success due to scattering and attenuative losses. The high frequency (HF, 3–30 MHz) and VHF (30–300 MHz) bands have good penetration through ice, with wavelengths longer than typical englacial water bodies encountered along the transmission path (asserted by Smeets and others, 2012).

The attenuation of electromagnetic waves in glacial ice is reported in the study of high-energy neutrinos (Barwick and others, 2005; Barrella and others, 2011) as *attenuation length* (L_α) in metres. This is related to *attenuation coefficient* (α) in decibels per metre by Eqn (2) (Barrella and others, 2011):

$$L_\alpha = \frac{1}{\ln \sqrt{10}^{\frac{\alpha}{20}}}. \quad (2)$$

We can rearrange and simplify Eqn (2) to convert attenuation length to attenuation coefficient in dB m⁻¹:

$$\alpha = \frac{20}{(\ln 10)L_\alpha}. \quad (3)$$

Some typical values of attenuation length are shown converted to dB per kilometre in Table 2.

Attenuation lengths determined experimentally vary slightly by frequency (Barwick and others, 2005), with lower frequencies generally having longer attenuation lengths (and hence lower attenuation coefficients). Mitigating against both free-space and ice-related losses therefore points towards the use of lower frequencies for radio links within ice. However, low frequencies imply long wavelengths, which in turn requires physically large antennas, as an efficient antenna needs to be at least $\frac{1}{4}$ of a wavelength long. The WiSe system at 30 MHz has a wavelength of 10 m and used half-wavelength dipole receiving antennas which were 5 m long (Smeets and others, 2012). Large antennas become impractical to work with in the field, and we had the additional challenge of needing to fit our transmitting antenna into the 120 mm diameter Cryoegg enclosure. Our previous work used 151 MHz (wavelength 2 m), which had given satisfactory performance and allowed the receiving antenna to be easily carried in the field. The very small size of the Cryoegg enclosure meant that there was limited value in going to higher frequencies as

the benefits of having a better-matched transmitting antenna were far outweighed by the additional free-space and ice-related losses. We therefore looked for a system that could operate in the VHF band (30–300 MHz).

For frequencies in the VHF range (30–300 MHz), the attenuation lengths reported (Barwick and others, 2005; Barrella and others, 2011) range from 200 to 3000 m. We took the worst-case figure of 200 m (43.4 dB km⁻¹) as our design criterion for working in warm, wet ice and 400 m (21.7 dB km⁻¹) as a conservative estimate for cold, dry ice (Table 2).

Methods

Choice of transmission scheme

The term ‘transmission scheme’ encompasses all the technical aspects of the radio link – the modulation, error corrective coding, packetisation and higher-level protocols. We required a commercially available system designed for long battery life and for sending small amounts of data over long distances, often sold as low-power wide-area networks or ‘Internet of things’ systems. We selected Wireless M-Bus mode N1 (European Committee for Standardisation, 2013), which is intended for use in utility metering. It is designed to offer very long battery life and sends data at 2.4 kbit s⁻¹. It incorporates error corrective coding, which ensures that data received over the link do not contain errors introduced in transit, and supports optional cryptographic protection for security. It operates on the 169 MHz frequency band, which is available for general license-free use in Europe (CEPT ECC Recommendation 70-03). Wireless M-Bus is an open standard and a number of manufacturers provide implementations of it. This gives confidence that the technology will remain available, whereas a proprietary system carries a risk of the product being discontinued.

The Radiocrafts RC1701HP-MBUS4 modem used provides 0.5 W (27 dBm) power output on the 169 MHz band (Radiocrafts, Oslo, Norway). One module is fitted to the printed circuit board (PCB) inside Cryoegg, configured as a transmitter. For the receiver, we use Radiocrafts RC1701HP-MBUS4 demo kit with one board configured as a receiver. This board connects to a PC and outputs the decoded data received over the radio link. A Python script running on the PC applies a timestamp to the received packet data and records it in a log file. This approach avoids the need to have a source of accurate time on board Cryoegg.

Antenna selection

The transmitting antenna inside Cryoegg is constrained by the physical size of the spherical case. We chose the HA.10 from Taoglas which is designed for the 169 MHz band, consisting of a pair of 30 mm long air-cored helical elements and a matching network. To minimise the use of conductive materials around the antenna, the upper hemisphere is devoted to the antenna and the remaining electronics fit into the lower hemisphere (Fig. 1a).

The receiving antenna on the surface provides additional gain to the system to help overcome the attenuation through the ice, and to compensate for the small size of the transmitting antenna – an ideal antenna would be 450 mm long, yet Cryoegg’s diameter is only 120 mm. We elected to use a pair of crossed Yagi-Uda antennas (InnovAntennas, Canvey Island, UK), which provide a gain of ~8 dB individually. They are combined through a 90° hybrid combiner (part number ZMSCQ-2-180BR+, Mini-Circuits, Brooklyn, NY, USA) which makes them behave as a single circularly polarised antenna, but at the expense of 3 dB loss in the combiner. By transmitting with linear polarisation and receiving with circular polarisation, we make the radio link performance relatively

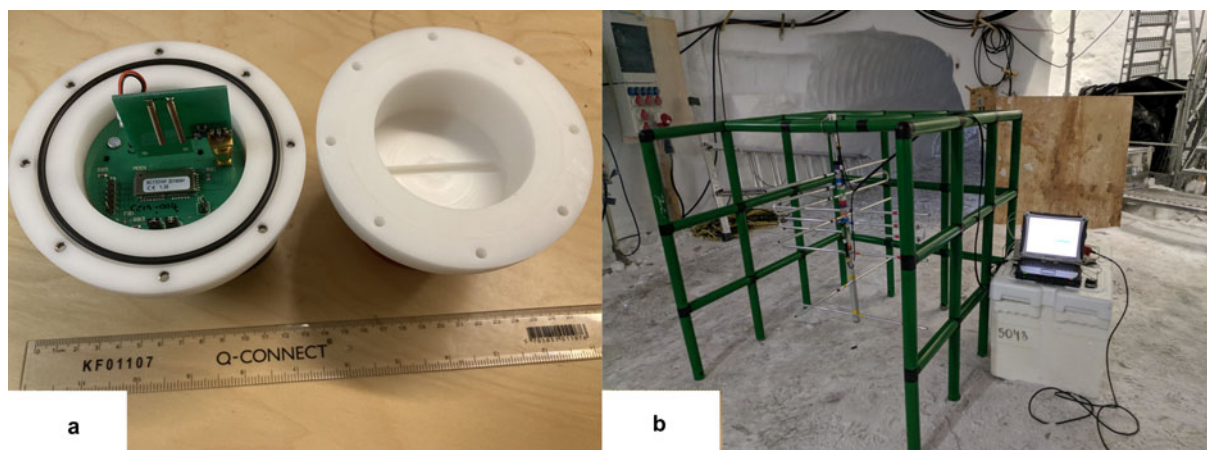


Fig. 1. (a) Cryoegg with upper casework removed; (b) receiving antenna mounted on plastic frame.

independent of Cryoegg's orientation. This technique was also used by the WiSe project team (Smeets and others, 2012).

The receiving antenna is 1 m long. In order to minimise disturbance to the antenna pattern caused by metal parts close to the antenna elements, we used a modular plastic frame (Quadro, Hamburg, Germany) to support the antenna (Fig. 1b).

The radiation pattern of Cryoegg was assessed in a screened RF test chamber (at the Wolfson Centre for Magnetics in Cardiff) lined with absorbent ferrite material to prevent multipath. A log-periodic antenna was used to receive the signal and the signal level was observed using a spectrum analyser in peak hold mode.

Link budget

A link budget is used to evaluate whether an attenuation-limited radio link will work in practice. Starting with the power output of the transmitter, gains and losses in the system are totalled up and compared to the sensitivity of the receiver. To allow some margin for unexpected attenuation, we aim for a received power level several dB higher than the sensitivity. Link budgets are traditionally calculated in decibel units as this allows the gains and losses to be added and subtracted (rather than multiplied and divided). Hence we use decibel units of power, such as dBW: decibels relative to 1 W ($0 \text{ dBW} = 1 \text{ W}$) or dBm: decibels relative to 1 mW ($0 \text{ dBm} = 1 \text{ mW} = -30 \text{ dBW}$, and $+30 \text{ dBm} = 1 \text{ W} = 0 \text{ dBW}$).

The link budget calculation (Table 3) assumes a 2000 m borehole through cold ice, with the attenuation coefficient estimated at 21 dB km^{-1} . The performance of the transmit antenna was relatively poor, and so we estimated its gain at -15 dBi (dB relative to an isotropic antenna) based on data from the manufacturer. For the 2000 m example shown here, the received signal margin is 10.5 dB.

Sensors

The Keller PA-20D pressure sensor (max. 250 bar; Keller, Winterthur, Switzerland) has a vacuum-sealed membrane and communicates with the microcontroller via the digital I²C interface (Inter-Integrated Circuit; UM10204 I²C-bus specification and user manual, 2014). It provides internal temperature compensation, and supplies a temperature reading alongside the pressure reading, although the manufacturer does not guarantee its performance at temperatures below 0°C . Hence we provided our own independent temperature sensor (details below). The sensor provides a 16-bit pressure reading to the microcontroller but uses only half the available range (the rest being used to allow it to report pressures slightly beyond the calibrated range). This means that the smallest

Table 3. Link budget calculation for Cryoegg in 2000 m borehole in cold ice (gains are positive values, losses are negative)

			Link budget contribution	Units
Transmitter power	0.5	W	27.0	dBm
Coupling loss			-0.5	dB
Transmit antenna gain			-15.0	dBi
Distance to receiver	2	km		
Frequency	169	MHz		
FSPL			-83.0	dB
Attenuation coefficient for cold ice	21	dB/km		
Ice-related loss			-42.0	dB
Cross-polarisation loss			-3.0	dB
Receive antenna gain			8.0	dBi
Total power at receiver			-108.5	dBm
Receiver sensitivity	-119	dBm		
Margin			10.5	dB

pressure step reportable is 7.6 millibars. The nominal total error band is 1% of full scale, i.e. 2.5 bar, but in practice we found we could reliably record changes in water pressure down to 0.1 bar (1 m hydrostatic pressure) during field experiments.

The temperature and EC sensors are adapted from earlier designs (Bagshaw and others, 2012, 2014). The EC sensor consists of a square wave oscillator which supplies a 500 Hz waveform to a potential divider consisting of a precision resistor and a pair of sense electrodes. The sense electrodes are a pair of M3 stainless steel hex-headed bolts that protrude through the case. The AC waveform from the midpoint of the potential divider passes through a precision rectifier and RC filter to produce a DC voltage that varies inversely with EC between the sense electrodes. This is sampled by the microcontroller's analogue-to-digital converter (ADC) and the resulting digital value is reported over the radio link. The temperature sensor is a Pt1000 platinum resistance device, used in a full-bridge configuration with three fixed resistors. It is driven by a current source and measured using an instrumentation amplifier, with the output fed to the microcontroller's ADC. Cryoegg reports the digital value from the ADC over the radio link, allowing calibration to be carried out externally. The Pt1000 resistor is mounted to the back of one of the EC sense electrodes with a thermal pad, ensuring that it has thermal but not electrical contact.

Microcontroller selection

To maximise battery life, Cryoegg has a 'sleep' mode where most subsystems were powered down between measurements. The

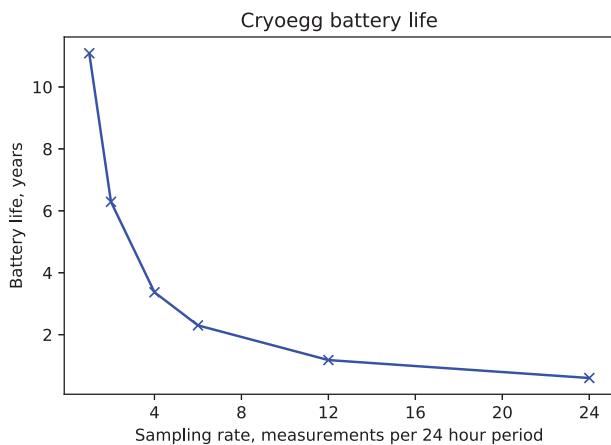


Fig. 2. Cryoegg projected battery life with varying sampling rate.

STM32L433RCT6P microcontroller (STMicroelectronics, Geneva, Switzerland) has a built-in Real Time Clock module (RTC) which uses an external quartz crystal oscillator to provide reliable timekeeping at very low power. This ‘wakes’ the microcontroller when it is time for the next measurement. The RTC draws ~ 500 nA at 3.3 V with the rest of the microcontroller shut down. The microcontroller has a 32-bit ARM Cortex M4 processor that can be clocked at up to 80 MHz, 256 kB of flash memory and 64 kB of RAM, and includes the ADC for the temperature and EC sensors; I²C interface for the pressure sensor; and Universal Asynchronous Receiver/Transmitter (UART) for communicating with the radio module. It also controls several power switches that enable and disable power to other parts of the circuit.

Power supply design and power consumption

The radio modem module has relatively high power consumption during transmit – requiring 500 mA at 3.3 V for <500 ms during each transmission, which puts a lot of demand on the battery and power supply to be able to supply this peak current. A lithium-polymer rechargeable pouch cell can supply sufficient peak current and be recharged between tests. The battery selected has a 3.7 V nominal voltage and a capacity of 400 mAh.

A regulator IC with an enable input (NCP115ASN330T2G, ON Semiconductor, Phoenix, AZ, USA) supplies 3.3 V to the sensors when enabled, and also provides the ADC reference voltage to the microcontroller. Other parts of the circuit are supplied with unregulated battery voltage.

To estimate the battery life, we measured the power consumption of Cryoegg during transmission and during sleep mode in the laboratory, using a logging multimeter (Mooshimeter, Mooshim Engineering, San Francisco, CA, USA) that could measure voltage and current from the battery simultaneously. The measure-and-transmit cycle takes 3.2 s and consumes 0.5 J. The sleep mode current consumption proved to be too low for the meter to measure (the lowest current it can record is 5 μ A). We therefore assume that the sleep mode current consumption is that of the microcontroller only (since everything else is disabled) and take the value quoted in the microcontroller datasheet of 500 nA.

The projected battery life based on these measurements is over 6 years at two measurements per day. Even allowing for some self-discharge in the battery, this gives scope to increase the measurement frequency. A measurement every 2 h (i.e. 12 times per day) gives a battery life of just over a year. Battery life estimates at different sampling rates are shown in Figure 2. Table A1 in Appendix A shows an example of battery life calculation in more detail.

Mechanical design

We aimed to provide a simple and robust mechanical design that was straightforward to assemble for testing. The spherical case-work is machined in two halves from acetal copolymer, a hard engineering plastic (Fig. 1a). The sensor PCB sits directly onto the bottom of the cylindrical internal void and is secured in place by two M3 threaded spacers, then potted with Magic Rubber (Raytech, Settimo Milanese, Italy). There are two further PCBs that mount above the sensor PCB, which interconnect using multiway connectors. The processor PCB contains the microcontroller and associated components, and also provides mechanical support for the battery. The radio PCB is uppermost and supports the radio module, antenna connector, battery connector and headers for programming and debugging. The pouch cell battery is sandwiched in the gap between the radio and processor PCBs. The antenna PCB connects to the radio PCB via an SMA connector and is supported by a groove in the crown of the upper hemisphere. This design allows the upper hemisphere to be easily removed for access to the electronics, and to connect the battery before deployment. The upper and lower hemisphere seal with a rubber O-ring and are held in place by eight machine screws.

Software

The software on the Cryoegg microcontroller is written in C, using the STM32 Hardware Abstraction Libraries. The software goes through the following steps:

- Power up the sensors
- Make measurements
- Power down the sensors
- Power up the radio module
- Pack the sensor data into a data packet
- Send the data packet to the radio module to be transmitted
- Power down the radio module
- Set the sleep timer for the next measurement
- Enter deep sleep (‘SHUTDOWN’) mode

On awakening from SHUTDOWN mode, the program restarts from the beginning, thus giving an endless loop. The measurements are transmitted immediately after being made, and no data are stored on Cryoegg, since we do not expect to retrieve Cryoegg after deployment.

Field testing

We conducted three field tests during July and August 2019 at two sites in Greenland (The East Greenland Ice core Project (EastGRIP) drill site and Sermeq Kujalleq/Store Glacier) and one in Switzerland (Rhône Glacier). The objectives of the field tests were to verify the operation of Cryoegg and its receiver in a real glacial environment. We wanted to demonstrate the operation of the radio link in both cold deep ice and shallower temperate ice, and confirm the mechanical integrity of the device when subjected to hydrostatic pressure in fluid-filled boreholes.

East Greenland ice core project site (EastGRIP)

EastGRIP is located at N75°38.05' W036°00.22' on the North East Greenland Ice Stream (NEGIS), the largest ice stream in Greenland, which drains 340 000 km² of the ice sheet and extends for over 1000 km inland (Fig. 3). Approximately 150 km from the onset, it reaches speeds of 65 m a⁻¹ (Joughin and others, 2010; Karlsson and Dahl-Jensen, 2015). EastGRIP is a unique project drilling an ice core into 2.5 km of fast-flowing ice to investigate ice stream beds (www.eastgrip.org). In summer 2019, the core

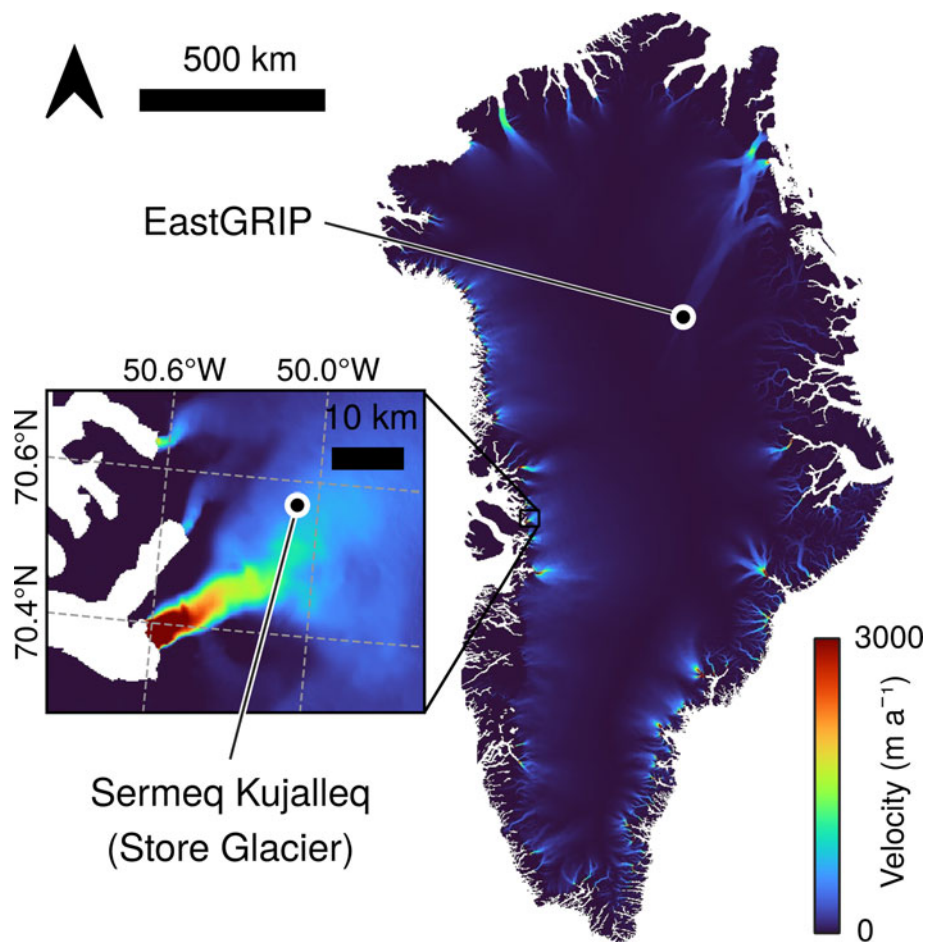


Fig. 3. Velocity map of Greenland ice sheet flow, showing locations of EastGRIP and Sermeq Kujalleq (Store Glacier) test sites in fast-flowing ice. Data from MEaSURES dataset of annual Greenland velocity for 2018 (Joughin and others, 2010; Joughin, 2017).



Fig. 4. Cryoegg ready for deployment on the EastGRIP ice core winch.

had been drilled to 2 km depth, leaving behind a 2 km borehole filled almost completely with drill fluid. The purpose of our field trial at this site was to obtain a range test for the radio link and a pressure test for the mechanical design. Cryoegg was deployed in a mesh bag and attached to the main winch (Fig. 4). The orientation of Cryoegg within the bag was not fully controlled due to its spherical shape, although the pressure sensor protruding through the mesh helped to prevent it from shifting. The receiving antenna was set up in the drill trench, close to the winch (Fig. 1b). Cryoegg was lowered and raised into the borehole several times and the received signal strength

(RSSI) and live data stream monitored at the surface, adjacent to the top of the borehole.

Responder site at Sermeq Kujalleq (Store Glacier)

We tested Cryoegg at an inland site (N70°33.889' W50°04.558') at Sermeq Kujalleq (Store Glacier), the third fastest outlet glacier in West Greenland (Fig. 3). It has a catchment of 35 000 km² that includes supraglacial lakes that periodically drain via cracks and moulins, several on an annual basis (Chudley and others, 2019). The glacier experiences changes in ice flow associated with sudden injections of meltwater to the pressurised drainage system (Doyle and others, 2018), but the link between surface lake drainage and the subglacial hydrology is poorly defined, primarily because instrumenting a draining lake with cabled sensors is near-impossible. There is extensive supporting data available on the subglacial bed structure, lake drainage frequency and ice strain rates (Hofstede and others, 2018; Young and others, 2018; Chudley and others, 2019). Sermeq Kujalleq (Store Glacier) is the site of the RESPONDER project ('Resolving Subglacial Properties, hydrological networks and dynamic evolution of ice flow on the Greenland Ice Sheet', <https://www.erc-responder.eu/>), offering access to the glacier bed through hot water drilling. The ice is ~1 km thick at this site (Morlighem and others, 2017) and moving at 600 m a⁻¹ (Chudley and others, 2019). Bed access holes were hot water drilled in July 2019.

A surface propagation test assessed the range of data transmission through air by monitoring the RSSI and live data stream as the receiving antenna was deployed at a fixed site and Cryoegg hand-carried over a distance of 1.6 km. A hand-held GPS receiver was used to record the position of Cryoegg as it was carried, and the fixed position of the Cryoegg receiver.



Fig. 5. Topographic map of Switzerland showing the location of the Rhône Glacier.

Rhône glacier site

The Rhône Glacier is located at N46°34.32' E8°22.58' in the Swiss Alps (Fig. 5). It is one of the most studied glaciers, with records of front position dating back to the 17th century (Church and others, 2019). The 16 km² glacier is at the pressure melting point throughout and there is an active subglacial drainage network. The glacier is the focus of an intensive subglacial monitoring project, with artificial moulines drilled via hot water in 2018. The moulines remained active in August 2019, when we deployed Cryoegg on the end of a rope tether.

Salt dilution gauging (Moore, 2005) was used to estimate moulin discharge. A known quantity of tracer, sodium chloride (NaCl, 'table salt') was added to the supraglacial stream ~25 m upstream of the moulin. The discharge can then be calculated from EC readings and the concentration of NaCl added. EC was measured in the supraglacial stream by a Keller DCX-22-CTD 15 m upstream of the moulin and also recorded and transmitted once per second by a Cryoegg lowered into water at the bottom of the moulin.

Results

Laboratory RF tests

RF power meter assessments confirmed the assumption (Table 3) that the transmitter put out the full +27 dBm (0.5 W) during each transmission.

The horizontal radiation pattern was measured at eight points around the circumference and is shown in Figure 6. For this measurement, the receiving antenna (a log-periodic) was vertically polarised (a brief check showed that this gave a larger signal than when horizontally polarised) and Cryoegg was orientated with its case split line horizontal. Two complete revolutions were measured to check the consistency. The pattern is largely omnidirectional, with <2 dB of variation between all the measurements.

To simulate the RF performance in the borehole, we re-oriented the Cryoegg to have the same orientation as it would have in the borehole, with the split line vertical and normal to the receiving antenna boresight – i.e. with the crown of the upper half pointing towards the receiving antenna, and the sensor ports pointing away. The receiving antenna was vertically polarised. The results in Figure 7 show that the signal level is significantly lower (10–12 dB) than in the horizontal plane, and that the pattern is not omnidirectional; there is a 6 dB variation as the unit is rotated.

Surface propagation at Sermeq Kujalleq (Store Glacier)

Figure 8a shows recorded signal strength for successfully received data packets against range from the receiver. The terrain profile in Figure 8b was produced from ArcticDEM v3 (<https://doi.org/10.7910/DVN/OHHUKH>) 2 m mosaic values extracted to match the GPS positions recorded in the field. A line-of-sight binary was calculated using the QGIS visibility analysis plugin with the receiver height set at 1.5 m and the transmitter height at 1 m.

Deployment at Sermeq Kujalleq (Store Glacier)

Cryoegg was lowered into a hot water drilled borehole and a moulin. One deployment attempt was made in the hot water drilled borehole, but the borehole proved too narrow for Cryoegg to pass through. One data point was obtained with Cryoegg in the borehole ~400 m below the surface, but it was impossible to proceed further because of borehole refreezing. Moulin deployment was attempted in a very large moulin (measured at 4.3 m³ s⁻¹ discharge at the time of deployment) adjacent to the drill site. Cryoegg was caught in a series of plunge pools and eventually the force of the water caused it to break free from its tether and it was rapidly swept away out of range. We only obtained a few data points before losing the signal.

Downhole propagation at EastGRIP

At EastGRIP, the borehole is filled with ESTISOL 240 drill fluid rather than water (Sheldon and others, 2014). Previous tests at the site (Bagshaw and others, 2018) demonstrated that the fluid had minimal impact on signal propagation. Figure 9 shows the RSSI plotted against depth. Depth is linearly interpolated between depth-measured winch halt points (shown as vertical gridlines on Fig. 9), which is a fair assumption because the winch motor speed was constant between these halts. The firmware was configured to produce a burst of 16 packets, one per second, and then wait for 60 s before the next burst. This accounts for the clustered data points in Figure 9, as all the successfully received packets are plotted. There are large variations (>10 dB) in signal level at 300, 400 and 500 m, coinciding with the point where the winch was halted, and even retrograde paths, for example, between 400 and 500 m; 700–850 m; 1000–1100 m. The deepest point at which packets were successfully received was 1340 m below the surface. No packets were received as Cryoegg was pulled back up to the surface.

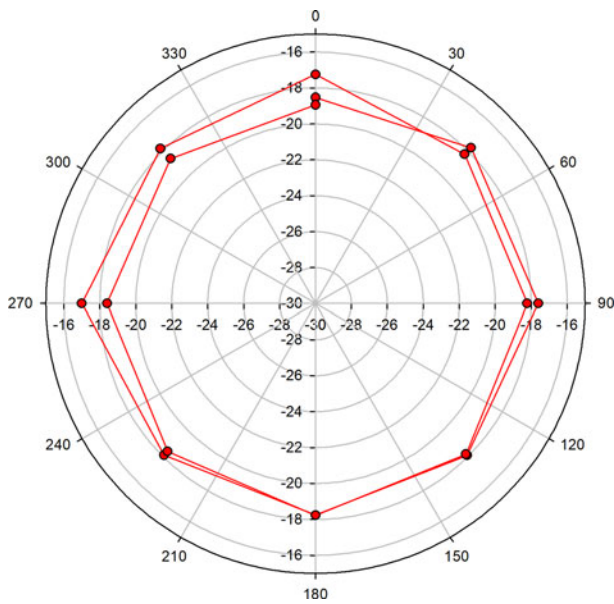


Fig. 6. Horizontal radiation pattern of Cryoegg measured in the RF test chamber.

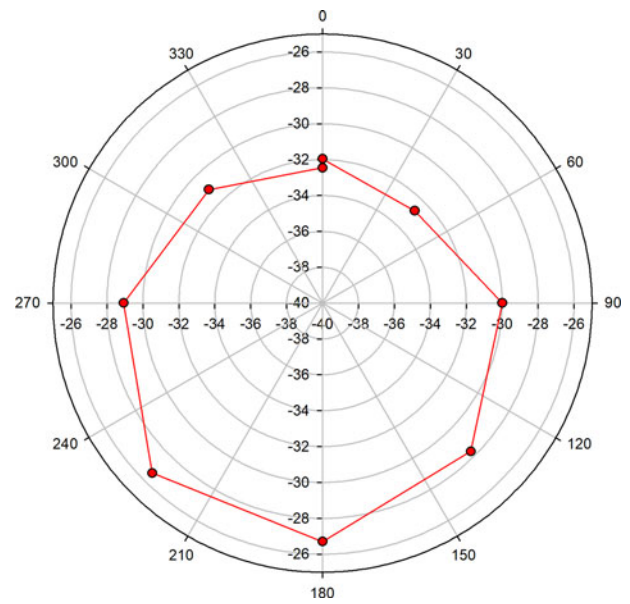


Fig. 7. Vertical radiation pattern of Cryoegg measured in the RF test chamber.

When Cryoegg was retrieved, it was found to be full of drill fluid, indicating that it had leaked under pressure.

The hydrostatic pressure increased with depth (Fig. 10) – the small offset is because the drill fluid is ~ 50 m below the surface level. Data were obtained down to 1340 m, although significant packet loss occurred beyond 1250 m. The two temperature plots represent data from the two different temperature sensors. The Pt1000 sensor is inside the case, hence it records a higher temperature for a given depth when compared with the Keller, which has direct contact with the drill fluid. The conversion equation from the Pt1000 reported value (which is in arbitrary units) to temperature is based on theory and has not been confirmed by calibration. Since the primary test objective was to test the radio link, we did not prioritise calibrating the temperature sensors prior to the field deployment. The high degree of clustering of the data points from the Keller sensor suggests that it contains some internal averaging, although this may be caused by the significant mass of the sensor body itself. Cryoegg was at ambient ice surface temperature before entering the borehole, so the majority of the temperature data recorded here is simply the instrument cooling down to the ambient englacial temperature. The spread in Pt1000 temperature results beyond 400 m depth is caused by self-heating of the sensor due to repeated measurements in quick succession, which becomes apparent once Cryoegg has cooled to the ambient englacial temperature.

Moulin drainage at Rhône glacier

Cryoegg did not reach the bed of the Rhône Glacier, 200 m below the surface, via the moulin and instead appeared to be in a deep plunge pool 150 m below the surface. Pressure readings received from Cryoegg in real time confirmed that it was in up to 25 m deep water. Figure 11 shows the pressure recorded while Cryoegg was in the plunge pool, and the corresponding RSSI. There was a sharp rise in pressure as Cryoegg was lowered into the water at 13:12:00 UTC and then a gradual decline over the next 40 min. The gap in the data centred on 13:55 was an interruption in the data logging. After the logging resumed, the water pressure had fallen to atmospheric pressure. The reduction in water pressure coincided with a 10 dB increase in RSSI over the same period.

Salt discharge gauging at Rhône glacier

The salt discharge gauging experiment at Rhône Glacier consisted of injecting a 100 g L^{-1} NaCl salt solution into a supraglacial stream, 25 m upstream from a moulin. A Keller DCX-22-CTD in the supraglacial stream, 10 m downstream from the injection point, measured the EC in the stream. Simultaneously, a Cryoegg in the moulin plunge pool (150 m below the ice surface) measured the EC and transmitted the measurements to the surface in real time.

Figure 12 shows the results from the Keller logger in the stream alongside the results from Cryoegg in the moulin.

The discharge of the supraglacial stream was calculated by the salt dilution as 104 L s^{-1} (Moore, 2005), and the discharge within the moulin was slightly higher at 113 L s^{-1} . The time between the two peaks was 60 s. The velocity of the water between the two instruments was 2.75 m s^{-1} based on the transit time and the distance between them (15 m in the stream + 150 m down the moulin = 165 m).

Discussion

Radioglaciological implications

Surface range test

The main objective of field testing was to verify the performance of Cryoegg in a real glacial environment. The surface range test at Sermeq Kujalleq/Store Glacier (Fig. 8) confirmed that the radiated output of Cryoegg matched our design calculations. We modelled the expected RSSI using the conventional two-ray ground-reflection model (Bullington, 1947) used for VHF propagation. The transmitter and receiver heights required were modelled using the DEM profile shown in Figure 8b. The transmitter and receiver parameters in the model were those from the link budget in Table 3. The model produces a good fit to the real data, confirming that the parameters were indeed realistic estimates. The variations in the signal strength data are because the DEM profile is derived from data with a 2 m resolution of the glacier surface terrain – but the glacier surface had undulations of ~ 0.5 –1 m in height. This caused variations in antenna height during the test that are not reflected in the DEM profile. The later part of the test was beyond the line of sight to the

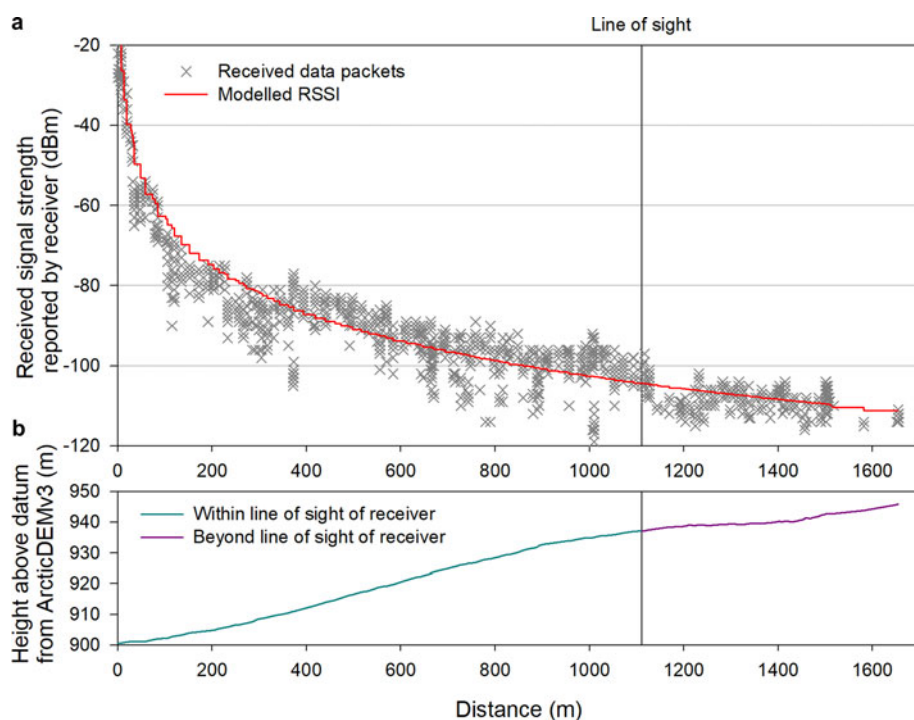


Fig. 8. (a) RSSI recorded by receiver during surface range test at Sermeq Kujalleq (Store Glacier) and modelled received signal strength. (b) The figure shows the ground elevation (height above the WGS84 ellipsoid) along the route taken. The black vertical line in both plots shows the point where the transmitter went beyond the line of sight to the receiver due to the ice sheet's surface topography.

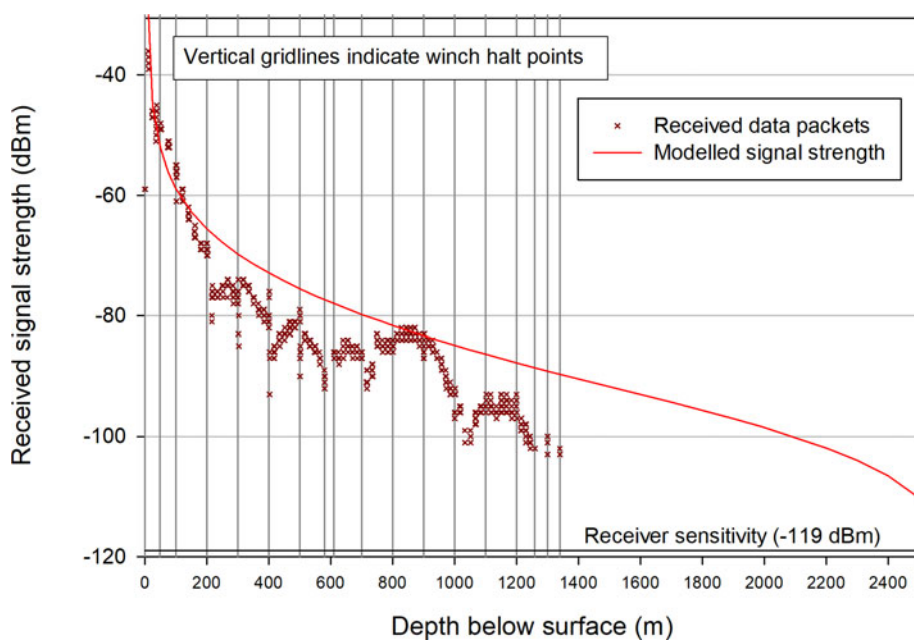


Fig. 9. Received signal strength of successfully-received data packets during a test in the EastGRIP borehole, together with modelled signal strength (explained in 'Radioglaciological implications' section).

receiver (as shown by the elevation profile in Fig. 8b), which accounts for the step reduction in signal strength beyond 1100 m.

EastGRIP borehole test

The test in the EastGRIP borehole was intended to verify both the mechanical and electrical performance of Cryoegg in a simulated deployment, and demonstrate the radio link through deep glacial ice. No data were received beyond 1340 m depth, and on return to the surface, Cryoegg was found to have failed and stopped transmitting. This appears to have been a mechanical failure. Drill fluid was found in the Cryoegg housing after the tests. The fluid is non-conductive and so should not have caused any electrical damage, but the hydrostatic pressure is likely to have affected some components. The most likely failure points are the battery (which being a soft 'pouch cell' type has no protection from pressure)

and its connectors, which may be forced apart by non-conductive fluid under high pressure, breaking the circuit.

An important question remains: if the leak had not occurred and Cryoegg had continued operating down to the bottom of the borehole (2000 m down), would we have received data at that depth? To determine this, we estimate the RF performance based on the recorded data.

The receiver sensitivity (the minimum decodable signal strength) is -119 dBm (1.25 fW), and in other range tests (Fig. 8), we succeeded in decoding signals down to this level (RC1701xx-MBUS Datasheet, 2018). However, the RSSI data for the EastGRIP borehole (Fig. 9) show that the weakest signals received were at -103 dBm, 16 dB above the minimum receivable level. This suggests the system would have continued working beyond 1340 m depth without the mechanical failure. To forecast

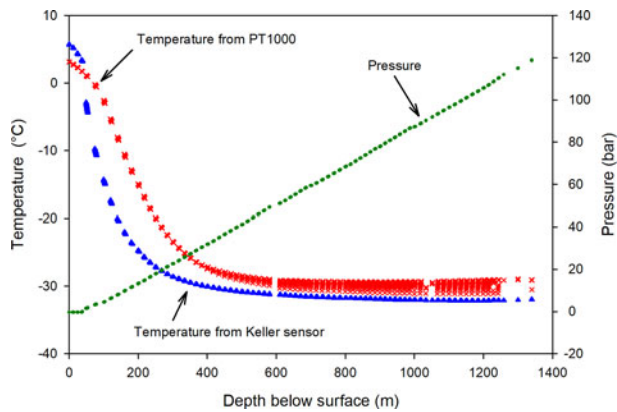


Fig. 10. Cryoegg sensor data received at the surface during deployment into the EastGRIP borehole.

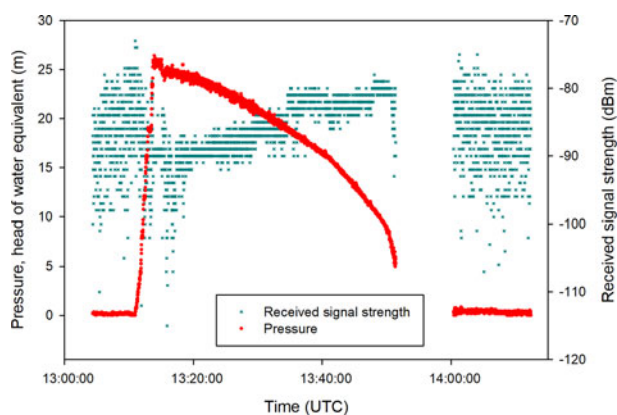


Fig. 11. Pressure and received signal strength from Cryoegg in a moulin on Rhône Glacier, 15th August 2019.

signal levels at greater depth, we modelled the expected RSSI in the borehole. The model is based on the same method as for the link budget in Table 3, but with ice attenuation calculated based on the glacier's internal temperature at each depth rather than assuming a constant value at all depths.

The temperature profile of the EastGRIP borehole was measured in July 2019 using the University of Copenhagen's automated logger (Gundrestrup and others, 1994). We applied the temperature measurements to an attenuation model (MacGregor and others, 2007, 2015) to give an estimate for the ice-related attenuation down to 2100 m below the surface (Fig. 9). To continue the temperature profile to the glacier bed depth (2500 m), we conjectured that the temperature would rise rapidly to reach 0°C at the bed, by analogy with the temperature profile at NorthGRIP (Dahl-Jensen and others, 2003). This represents a worst-case since the model produces very high attenuation (69 dB km^{-1}) at 0°C. This produces a profile with relatively low attenuation ($\sim 7 \text{ dB km}^{-1}$) in the coldest part of the glacier, increasing rapidly at the surface and bed where the ice is warmer.

When we initially developed the model, we found that using the value of -15 dBi for the transmit antenna gain (which produced a good fit to the surface range test data) overestimated the RSSI in the borehole, even at points very close to the surface. This suggests that the radiated signal from Cryoegg was much lower in the borehole when compared to the surface range test. It is likely that the antenna performance was affected by the substantial metal apparatus on the winch cable just above where Cryoegg was attached. The dielectric constant of the drill fluid is not the same as in air and this may also have affected the

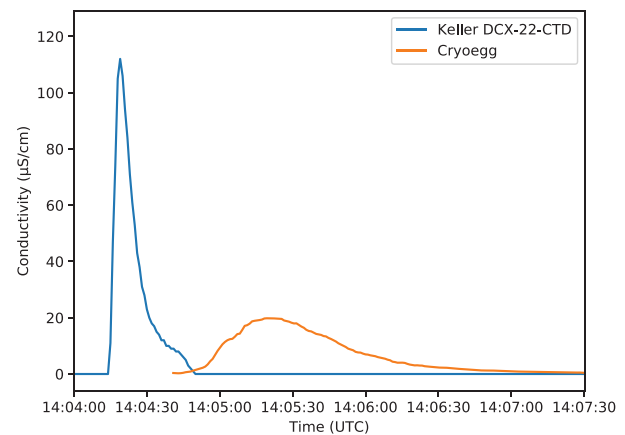


Fig. 12. Comparison of salt wave passing Keller logger in the supraglacial stream with Cryoegg within the moulin, 15th August 2019.

antenna matching. Consequently, we reduced the transmit antenna gain by 20 dB (to -35 dBi) in the model to produce a result that more closely fits the observed data. The final model output with the reduced transmit gain is plotted in Figure 9.

The modelled signal strength is higher than the real data at most depths (Fig. 9), although it matches the peak between 800 and 900 m, and there are two further effects that help explain why.

Firstly, the large ($>10 \text{ dB}$) variation in signal strength observed at several winch halt points is most likely caused by Cryoegg rotating on the vertical axis as the wire rope twists. Cryoegg was oriented with its split line horizontal during these tests, meaning that the transmitting antenna is oriented in an end-fire mode towards the receiver. The deceleration of the winch will result in some of the momentum of Cryoegg and the cable being converted into torsional forces on the winch cable, with Cryoegg twisting back and forth on the end of the cable. This will affect the radiation from the antenna because the radiation pattern seen by the receiving antenna is not uniform (Fig. 7). It is plausible that the retrograde slope of the signal strength between 400 and 500 m is caused by Cryoegg slowly rotating on the winch cable, given the signal variation is comparable to that seen during the 400 and 500 m winch halts.

Secondly, birefringence likely impacted the signal. Birefringence is a phenomenon exhibited by many crystalline materials, where the refractive index varies depending on the polarisation and direction of propagation of electromagnetic waves. Glacier ice affects the polarisation of VHF radio waves through birefringence, and radar studies use this effect to infer details about the crystal fabric of the glacier ice (Hargreaves, 1978; Li and others, 2018). Birefringence splits the wave from Cryoegg into two elliptically-polarised waves of opposing chirality with differing phase velocities. The relative phase delay between the two waves appears at the receiver as an apparent change in polarisation, and therefore it is possible that the wave could arrive at the receiving antenna on the opposite polarisation to the antenna, resulting in a 'null' – a significant reduction in RSSI. Since this phase delay relates to distance travelled through the medium, this effect would produce nulls at specific depths corresponding to relative phase delays of 180 degrees. The signal strength plot (Fig. 9) appears to show a number of nulls – notably at ~ 600 and 1040 m , which are most likely caused by birefringence. Multipath reflection effects, such as when the signal reflected off a surface interferes destructively with the direct signal at the receiver (Griffiths, 1987, 102–104), are the other possible explanation, but these can be discounted because there is no obvious candidate for the reflecting surface. The geometry required to produce widely-spaced large nulls rules out horizontal reflectors

like the glacier bed or internal layers, and the shear margin is too far away (5 km) to produce this type of null.

The axial rotation of Cryoegg and the birefringent effects may also act in concert, which would explain why the signal variations are so large at some of the winch halt points (>10 dB at most locations). These two effects explain why the signal level drops below the modelled values: the model assumes constant antenna gain and matched polarisation, whereas in the real data, the orientation varies (altering the transmit antenna gain) and the birefringence means that a proportion of the signal power is transferred to the opposite polarisation and is lost to the receiver.

The birefringent effect could be mitigated against in future development by feeding the output of each of the two crossed receiving antennas into a two-channel diversity receiver, which would then be able to decode the signal regardless of its polarisation. This polarisation diversity technique has previously been demonstrated mitigating polarisation nulls in HF ionospheric radio links (Stott, 2005) where magnetoionic effects produce polarisation changes which are analogous to those produced by birefringence (Davies, 1990).

Rhône glacier moulin test

The performance of the radio link in the Rhône glacier moulin (Fig. 11) was satisfactory. We anticipated that the temperate ice and presence of flowing water would increase the overall attenuation. Figure 11 shows that the signal propagating through 25 m of meltwater and a further 125 m of temperate ice to the glacier surface was attenuated to -90 dBm. This compares with the EastGRIP borehole (Fig. 9) where this signal strength was reached after more than 500 m. The reduction in observed moulin water pressure, indicative of 25 m head of water draining out of the moulin, produced an increase in RSSI by ~ 10 dB. This confirms that the presence of liquid water increases the signal attenuation.

The variation in signal is much greater when Cryoegg is in the 'atmospheric pressure' region of the moulin rather than when it is in >1 m of water (Fig. 11). When Cryoegg is reporting pressure close to atmospheric pressure, it is being splashed by the water, or water is flowing smoothly past it. In this scenario, the water flow will spin and agitate Cryoegg on the end of the rope, creating variation in signal level because of the antenna pattern. The turbulent flow of the water will also create ever-changing levels of attenuation. However, once Cryoegg is below the water surface, the viscosity of the water will reduce its spinning and agitation, and the attenuation due to the water will be constant.

Glaciohydrological implications

The water pressure recorded by Cryoegg in the moulin steadily decreased during the 40 min that it remained in the plunge pool (Fig. 11). Eventually, the water level dropped below the Cryoegg and it returned to atmospheric pressure with the characteristic fluctuations in RSSI caused by splashing water. We interpret this as dynamic drainage of the plunge pool over the afternoon, as glacier backed up in the drainage system forces its way to the glacier bed. Similar pressure variations have been previously observed in moulins (Iken, 1972; Röthlisberger, 1980; Holmlund and Hooke, 1983) and demonstrate that the subglacial drainage system is not in equilibrium but constantly fluctuating (Röthlisberger and Lang, 1987). The characteristic step-pool system develops if the moulin persists for more than one season (Gulley, 2009); the artificial moulin was drilled directly to the end in 2018, but by 2019 was 'kinked' and a plunge pool formed ~ 50 m above the bed.

Simultaneous salt tracing in a supraglacial stream feeding the moulin and within the moulin itself shows (Fig. 12) that the moulin discharge was slightly higher than the stream discharge –

unsurprising, as the stream that we measured was not the sole supply of water feeding the moulin. This experiment demonstrates Cryoegg's potential for measuring hydrological parameters in locations that are difficult to access. Previously, moulin discharge has been estimated at the surface (either by field measurements or remote sensing), which masks the effect of water being stored within the vertical column of the moulin itself (Werder and others, 2010). We show that it is possible to monitor supraglacial discharge, the height of the stored water column within the moulin, and the moulin discharge simultaneously and in real time, providing a valuable new approach for future studies of glacier hydrology.

Comparison with other wireless subglacial probes

The most successful wireless subglacial probe for deep ice has been the WiSe system (Smeets and others, 2012). This was demonstrated returning a signal through 2500 m of ice in Greenland. This system operated at 30 MHz in order to benefit from lower free-space path loss, but at the expense of making the antennas very large. The WiSe system suffered from some sky-wave interference affecting signal reception, which is a particular issue at 30 MHz and below, and required use of a large (5 m long) HB9CV type antenna to mitigate against it. WiSe required a 1 W ($+30$ dBm) transmitter to communicate at depths of more than 2000 m, but it is not clear how much of this power was actually radiated – the ferrite-loaded antenna used was likely to be very lossy.

The GlacsWeb system originally operated at 433 MHz (Martinez and others, 2004) but later (Martinez and others, 2013) used 151 MHz, giving a maximum reported range in ice of 70 m (Hart and others, 2019). Cryoegg is specifically designed for deep ice, and hence its radio performance greatly exceeds that of GlacsWeb, enabling its use in at least 1000 m of ice. Our probe and receiving antenna are both more compact than the WiSe system and we use commercially-available radio modules that adhere to an international open standard, which means that the key components are likely to be readily available well into the future.

Conclusion and outlook

We have undertaken a full re-design of the wireless subglacial sensor platform Cryoegg, using a new radio link technology and improved link budget design, and demonstrate that it can transmit sensor data in real time through more than 1.3 km of cold ice. Deployments in moulins in temperate ice show that Cryoegg is a valuable tool for recording englacial and subglacial hydrological properties in situ, and hence giving further insight into processes in these environments. The EC sensor, originally intended as a proxy for total dissolved solids in subglacial water, can facilitate salt dilution gauging for real-time estimates of discharge. All sensors operated well, revealing englacial conditions and demonstrating their applicability for future subglacial deployments. The sensors fitted to the existing design were chosen because of their ease of implementation and their applicability to studies of subglacial hydrology, but Cryoegg can be adapted to support other sensors.

Future developments will refine and enhance the design, particularly with respect to the antenna performance and mechanical design, so that we have a robust instrument capable of returning data for months or years through 2.5 km of ice. This would enable us to match the performance of the WiSe system (Smeets and others, 2012) but with more compact antennas, enabling the Cryoegg to 'roam' through englacial and subglacial hydrological systems to collect spatially and temporally distributed measurements, reported in real time. Cryoegg technology will also be

adapted for englacial studies in irregular and refreezing hot-water-drilled boreholes, by creating a cylindrical form factor with a much smaller diameter than Cryoegg, allowing deployment in a smaller borehole.

Acknowledgements. This work was funded by UK Engineering and Physical Sciences Research Council (EPSRC) New Investigator Award EP/R03530X/1, awarded to E.A.B. We thank all who assisted us in the field, in particular: Trevor Popp, Romain Duphil and the EastGRIP drill team; ‘Mickey’ MacKay, Eliza Dawson and Rob Law at the RESPONDER site; Lai Bun Lok, Jonathan Hawkins, the ETH Zürich VAW Glaciology team and the Swiss Air Force at the Rhône Glacier site. Phil Anderson gave us the use of the RF test chamber. We are grateful for in-kind contributions of equipment from Quadro and Radiocrafts. We thank the team at DGF Engineering for the machining of the caseworks, Protronix EMS Ltd for the rapid production of the electronics, and Justin Johnson of InnovAntennas for the custom design of the receiving antenna. Miles Gould provided assistance with the algebra for Eqn (3). We thank our anonymous reviewers for their helpful contributions and suggestions. EastGRIP is directed and organised by the Center of Ice and Climate at the Niels Bohr Institute. It is supported by funding agencies and institutions in Denmark (A. P. Møller Foundation, University of Copenhagen), USA (US National Science Foundation, Office of Polar Programs), Germany (Alfred Wegener Institute, Helmholtz Centre for Polar and Marine Research), Japan (National Institute of Polar Research and Arctic Challenge for Sustainability), Norway (University of Bergen and Bergen Research Foundation), Switzerland (Swiss National Science Foundation), France (French Polar Institute Paul-Emile Victor, Institute for Geosciences and Environmental Research) and China (Chinese Academy of Sciences and Beijing Normal University). B.H. acknowledges support for hot-water borehole drilling from HEFCW through a Capital Equipment Grant awarded to Aberystwyth University, and from the NERC through grant NE/K006126. The RESPONDER project is funded by a Consolidator Grant to P. C. from the European Research Council, under the European Union’s Horizon 2020 research and innovation programme (Grant 683043). T.R.C. was supported by a Natural Environment Research Council Doctoral Training Partnership Studentship (Grant NE/L002507/1). ArcticDEM was created from DigitalGlobe, Inc., imagery and funded under National Science Foundation awards 1043681, 1559691 and 1542736.

References

- Bagshaw EA and 7 others** (2012) E-tracers: development of a low cost wireless technique for exploring sub-surface hydrological systems. *Hydrological Processes* **26**(20), 3157–3160. doi: [10.1002/hyp.9451](https://doi.org/10.1002/hyp.9451).
- Bagshaw EA and 6 others** (2014) Novel wireless sensors for in situ measurement of sub-ice hydrologic systems. *Annals of Glaciology* **55**(65), 41–50. doi: [10.3189/2014AoG65A007](https://doi.org/10.3189/2014AoG65A007).
- Bagshaw E and 10 others** (2018) Utilising Wireless Sensor Technologies in Glaciology. *Paper presented at AGU Fall Meeting 2018*. Washington, DC. Available at <http://adsabs.harvard.edu/abs/2018AGUFM.C43D1823B>.
- Barrella T, Barwick S and Saltzberg D** (2011) Ross Ice Shelf in situ radio-frequency ice attenuation. *Journal of Glaciology* **57**(201), 61–66. doi: [10.3189/002214311795306691](https://doi.org/10.3189/002214311795306691)
- Barwick S, Besson D, Gorham P and Saltzberg D** (2005) South Polar in situ radio-frequency ice attenuation. *Journal of Glaciology* **51**(173), 231–238. doi: [10.3189/172756505781829467](https://doi.org/10.3189/172756505781829467)
- Bullington K** (1947) Radio propagation at frequencies above 30 megacycles. *Proceedings of the Institute of Radio Engineers* **35**(10), 1122–1136. doi: [10.1109/JRPROC.1947.232600](https://doi.org/10.1109/JRPROC.1947.232600)
- Chandler DM and 11 others** (2013) Evolution of the subglacial drainage system beneath the Greenland Ice Sheet revealed by tracers. *Nature Geoscience* **6**(3), 195–198. doi: [10.1038/ngeo1737](https://doi.org/10.1038/ngeo1737).
- Chu VW** (2014) Greenland Ice sheet hydrology: a review. *Progress in Physical Geography: Earth and Environment* **38**(1), 19–54. doi: [10.1177/0309133313507075](https://doi.org/10.1177/0309133313507075)
- Chudley TR and 6 others** (2019) Supraglacial lake drainage at a fast-flowing Greenlandic outlet glacier. *Proceedings of the National Academy of Sciences* **116**(51), 25468–25477. doi: [10.1073/pnas.1913685116](https://doi.org/10.1073/pnas.1913685116).
- Church G and 5 others** (2019) Detecting and characterising an englacial conduit network within a temperate Swiss glacier using active seismic, ground penetrating radar and borehole analysis. *Annals of Glaciology* **60**(79), 193–205. doi: [10.1017/aog.2019.19](https://doi.org/10.1017/aog.2019.19)
- Clarke GKC** (1987) Subglacial till: a physical framework for its properties and processes. *Journal of Geophysical Research: Solid Earth* **92**(B9), 9023–9036. doi: [10.1029/JB092iB09p09023](https://doi.org/10.1029/JB092iB09p09023)
- Dahl-Jensen D, Gundestrup N, Gogineni SP and Miller H** (2003) Basal melt at NorthGRIP modeled from borehole, ice-core and radio-echo sounder observations. *Annals of Glaciology* **37**, 207–212. doi: [10.3189/172756403781815492](https://doi.org/10.3189/172756403781815492)
- Davies K** (1990) *Ionospheric Radio (IEE Electromagnetic Waves Series, Vol. 31)*. London, UK: The Institution of Engineering and Technology.
- Doyle SH and 7 others** (2018) Physical conditions of fast glacier flow: 1. Measurements from boreholes drilled to the bed of Store Glacier, West Greenland. *Journal of Geophysical Research: Earth Surface* **123**(2), 324–348. doi: [10.1002/2017JF004529](https://doi.org/10.1002/2017JF004529).
- European Committee for Standardisation** (2013) EN 13757-4:2013 – communication systems for meters and remote reading of meters. Wireless meter readout (radio meter reading for operation in SRD bands). Available at <https://bsol.bsigroup.com/en/Bsol-Item-Detail-Page/?pid=0000000030249978>.
- Flowers GE** (2018) Hydrology and the future of the Greenland Ice Sheet. *Nature Communications* **9**(1), 2729. doi: [10.1038/s41467-018-05002-0](https://doi.org/10.1038/s41467-018-05002-0)
- Friis HT** (1946) A note on a simple transmission formula. *Proceedings of the Institute of Radio Engineers* **34**(5), 254–256. doi: [10.1109/JRPROC.1946.234568](https://doi.org/10.1109/JRPROC.1946.234568)
- Griffiths J** (1987) *Radio Wave Propagation and Antennas*. Hemel Hempstead, UK: Prentice-Hall.
- Gulley J** (2009) Structural control of englacial conduits in the temperate Matanuska Glacier, Alaska, USA. *Journal of Glaciology* **55**(192), 681–690. doi: [10.3189/002214309789470860](https://doi.org/10.3189/002214309789470860)
- Gundestrup NS, Clausen HB and Hansen BL** (1994) The UCPH borehole logger. *Memoirs of National Institute of Polar Research Special Issue* **49**, 224–233. Available at <https://ci.nii.ac.jp/naid/110000010330>.
- Hargreaves ND** (1978) The radio-frequency birefringence of polar ice. *Journal of Glaciology* **21**(85), 301–313. doi: [10.3189/S0022143000033499](https://doi.org/10.3189/S0022143000033499)
- Hart JK and 5 others** (2019) Surface melt driven summer diurnal and winter multi-day stick-slip motion and till sedimentology. *Nature Communications* **10**(1), 1–11. doi: [10.1038/s41467-019-09547-6](https://doi.org/10.1038/s41467-019-09547-6)
- Hoffman MJ and 9 others** (2016) Greenland Subglacial drainage evolution regulated by weakly connected regions of the bed. *Nature Communications* **7**(1), 1–12. doi: [10.1038/ncomms13903](https://doi.org/10.1038/ncomms13903).
- Hofstede C and 7 others** (2018) Physical conditions of fast glacier flow: 2. Variable extent of anisotropic ice and soft basal sediment from seismic reflection data acquired on Store Glacier, West Greenland. *Journal of Geophysical Research: Earth Surface* **123**(2), 349–362. doi: [10.1002/2017JF004297](https://doi.org/10.1002/2017JF004297).
- Holmlund P and Hooke RL** (1983) High water-pressure events in moulins, Storgläciären, Sweden. *Geografiska Annaler: Series A, Physical Geography* **65**(1–2), 19–25. doi: [10.1080/04353676.1983.11888070](https://doi.org/10.1080/04353676.1983.11888070)
- Hubbard BP, Sharp MJ, Willis IC, Nielsen MK and Smart CC** (1995) Borehole water-level variations and the structure of the subglacial hydrological system of Haut Glacier d’Arolla, Valais, Switzerland. *Journal of Glaciology* **41**(139), 572–583. doi: [10.3189/S0022143000034894](https://doi.org/10.3189/S0022143000034894)
- Iken A** (1972) Measurements of water pressure in moulins as part of a movement study of the white glacier, Axel Heiberg Island, Northwest Territories, Canada. *Journal of Glaciology* **11**(61), 53–58. doi: [10.3189/S0022143000022486](https://doi.org/10.3189/S0022143000022486)
- Iken A** (1981) The effect of the subglacial water pressure on the sliding velocity of a glacier in an idealized numerical model. *Journal of Glaciology* **27**(97), 407–421. doi: [10.3189/S0022143000011448](https://doi.org/10.3189/S0022143000011448)
- Iken A and Bindshadler RA** (1986) Combined measurements of subglacial water pressure and surface velocity of Findelengletscher, Switzerland: conclusions about drainage system and sliding mechanism. *Journal of Glaciology* **32**(110), 101–119. doi: [10.3189/S0022143000006936](https://doi.org/10.3189/S0022143000006936)
- Iken A, Echelmeyer K, Harrison W and Funk M** (1993) Mechanisms of fast flow in Jakobshavn Isbræ, West Greenland: part I. Measurements of temperature and water level in deep boreholes. *Journal of Glaciology* **39**(131), 15–25. doi: [10.3189/S0022143000015689](https://doi.org/10.3189/S0022143000015689)
- Joughin I** (2017) MEaSUREs Greenland Ice Velocity Annual Mosaics from SAR and Landsat, Version 1. Boulder, Colorado USA. NASA National Snow and Ice Data Center Distributed Active Archive Center. doi: [10.5067/OBXC75U7540](https://doi.org/10.5067/OBXC75U7540).
- Joughin I, Smith BE, Howat IM, Scambos T and Moon T** (2010) Greenland flow variability from ice-sheet-wide velocity mapping. *Journal of Glaciology* **56**(197), 415–430. doi: [10.3189/002214310792447734](https://doi.org/10.3189/002214310792447734)
- Kamb B** (1970) Sliding motion of glaciers: theory and observation. *Reviews of Geophysics* **8**(4), 673–728. doi: [10.1029/RG008i004p0673](https://doi.org/10.1029/RG008i004p0673)

- Kamb B** (1987) Glacier surge mechanism based on linked cavity configuration of the basal water conduit system. *Journal of Geophysical Research: Solid Earth* **92**(B9), 9083–9100. doi: [10.1029/JB092iB09p09083](https://doi.org/10.1029/JB092iB09p09083)
- Karlsson NB and Dahl-Jensen D** (2015) Response of the large-scale subglacial drainage system of Northeast Greenland to surface elevation changes. *The Cryosphere* **9**(4), 1465–1479. doi: [10.5194/tc-9-1465-2015](https://doi.org/10.5194/tc-9-1465-2015)
- Lewis C and 6 others** (2015) Airborne fine-resolution UHF radar: an approach to the study of englacial reflections, firn compaction and ice attenuation rates. *Journal of Glaciology* **61**(225), 89–100. doi: [10.3189/2015JG14J089](https://doi.org/10.3189/2015JG14J089).
- Li J and 8 others** (2018) Multi-channel and multi-polarization radar measurements around the NEEM site. *The Cryosphere* **12**(8), 2689–2705. doi: [10.5194/tc-12-2689-2018](https://doi.org/10.5194/tc-12-2689-2018).
- MacGregor JA and 5 others** (2007) Modeling englacial radar attenuation at Siple Dome, West Antarctica, using ice chemistry and temperature data. *Journal of Geophysical Research: Earth Surface* **112**, F03008. doi: [10.1029/2006JF000717](https://doi.org/10.1029/2006JF000717)
- MacGregor JA and 11 others** (2015) Radar attenuation and temperature within the Greenland Ice Sheet. *Journal of Geophysical Research: Earth Surface* **120**(6), 983–1008. doi: [10.1002/2014JF003418](https://doi.org/10.1002/2014JF003418).
- Martinez K, Basford PJ, Jager DD and Hart JK** (2013) Using a heterogeneous sensor network to monitor glacial movement. *Paper presented at 10th European Conference on Wireless Sensor Networks*. Available at <http://eprints.soton.ac.uk/348427/1/paper.pdf>.
- Martinez K, Ong R and Hart J** (2004) Glacsweb: a sensor network for hostile environments. 2004 *First Annual IEEE Communications Society Conference on Sensor and Ad Hoc Communications and Networks*, 2004. *IEEE SECON* 2004. 81–87. doi: [10.1109/SAHCN.2004.1381905](https://doi.org/10.1109/SAHCN.2004.1381905).
- Moore RD** (2005) Introduction to salt dilution gauging for streamflow measurement. Part 3: slug injection using salt in solution. *Streamline Watershed Management Bulletin* **8**(2), 1–6.
- Morlighem M and 31 others** (2017) Bedmachine v3: complete bed topography and ocean bathymetry mapping of Greenland from multibeam echo sounding combined with mass conservation. *Geophysical Research Letters* **44**(21), 11051–11061. doi: [10.1002/2017GL074954](https://doi.org/10.1002/2017GL074954).
- Ng FSL** (2000) Canals under sediment-based ice sheets. *Annals of Glaciology* **30**, 146–152. doi: [10.3189/172756400781820633](https://doi.org/10.3189/172756400781820633)
- Nienow PW and 6 others** (2005) Hydrological controls on diurnal ice flow variability in valley glaciers. *Journal of Geophysical Research: Earth Surface* **110**, F04002. doi: [10.1029/2003JF000112](https://doi.org/10.1029/2003JF000112).
- Nienow PW, Sole AJ, Slater DA and Cowton TR** (2017) Recent advances in our understanding of the role of meltwater in the Greenland Ice Sheet System. *Current Climate Change Reports* **3**(4), 330–344. doi: [10.1007/s40641-017-0083-9](https://doi.org/10.1007/s40641-017-0083-9)
- Nye JF** (1976) Water flow in glaciers: jökulhlaups, tunnels and veins. *Journal of Glaciology* **17**(76), 181–207. doi: [10.3189/S002214300001354X](https://doi.org/10.3189/S002214300001354X)
- Plewe LA and Hubbard B** (2001) A review of the use of radio-echo sounding in glaciology. *Progress in Physical Geography* **25**(2), 203–236. doi: [10.1177/030913330102500203](https://doi.org/10.1177/030913330102500203)
- Pritchard HD, Arthern RJ, Vaughan DG and Edwards LA** (2009) Extensive dynamic thinning on the margins of the Greenland and Antarctic ice sheets. *Nature* **461**(7266), 971–975. doi: [10.1038/nature08471](https://doi.org/10.1038/nature08471)
- RC1701xx-MBUS Datasheet** (2018) Radiocrafts AS, Oslo, Norway. Available at https://radiocrafts.com/uploads/rc1701xx-mbus_datasheet.pdf.
- Röthlisberger H** (1972) Water pressure in intra- and subglacial channels. *Journal of Glaciology* **11**(62), 177–203. doi: [10.3189/S0022143000022188](https://doi.org/10.3189/S0022143000022188)
- Röthlisberger H** (1980) Gletscherbewegung und Wasserabfluss. *Wasser, Energie, Luft* **72**(9), 290–294.
- Röthlisberger H and Lang H** (1987) Glacial hydrology. In Gurnell AM and Clark MJ eds. *Glacio-Fluvial Sediment Transfer: An Alpine Perspective*. Chichester, UK: Wiley, pp. 207–284.
- Schoof C** (2010) Ice-sheet acceleration driven by melt supply variability. *Nature* **468**(7325), 803–806. doi: [10.1038/nature09618](https://doi.org/10.1038/nature09618)
- Sheldon SG, Steffensen JP, Hansen SB, Popp TJ and Johnsen SJ** (2014) The investigation and experience of using ESTISOL™ 240 and COASOL™ for ice-core drilling. *Annals of Glaciology* **55**(68), 219–232. doi: [10.3189/2014AoG68A036](https://doi.org/10.3189/2014AoG68A036)
- Smeets CJP and 6 others** (2012) A wireless subglacial probe for deep ice applications. *Journal of Glaciology* **58**(211), 841–848. doi: [10.3189/2012JG11J130](https://doi.org/10.3189/2012JG11J130).
- Sole AJ and 6 others** (2011) Seasonal speedup of a Greenland marine-terminating outlet glacier forced by surface melt-induced changes in subglacial hydrology. *Journal of Geophysical Research: Earth Surface* **116**, F03014. doi: [10.1029/2010JF001948](https://doi.org/10.1029/2010JF001948).
- Stott J** (2005) BBC R&D White Paper WHP 109: Digital Radio Mondiale: DRM, digital radio on long, medium and short waves – another radio revolution?. Available at <http://downloads.bbc.co.uk/rd/pubs/whp/whp-pdf-files/WHP109.pdf>.
- Tedstone AJ and 5 others** (2015) Decadal slowdown of a land-terminating sector of the Greenland Ice Sheet despite warming. *Nature* **526**(7575), 692–695. doi: [10.1038/nature15722](https://doi.org/10.1038/nature15722)
- Tranter M and 5 others** (2002) Geochemical weathering at the bed of Haut Glacier d’Arolla, Switzerland – a new model. *Hydrological Processes* **16**(5), 959–993. doi: [10.1002/hyp.309](https://doi.org/10.1002/hyp.309)
- UM10204 I2C-bus specification and user manual** (2014) NXP Semiconductors, Eindhoven, Netherlands. Available at <https://www.nxp.com/docs/en/user-guide/UM10204.pdf>.
- van den Broeke MR and 7 others** (2016) On the recent contribution of the Greenland ice sheet to sea level change. *The Cryosphere* **10**(5), 1933–1946. doi: [10.5194/tc-10-1933-2016](https://doi.org/10.5194/tc-10-1933-2016).
- Walder JS** (1986) Hydraulics of subglacial cavities. *Journal of Glaciology* **32** (112), 439–445. doi: [10.3189/S0022143000012156](https://doi.org/10.3189/S0022143000012156)
- Werder MA, Schuler TV and Funk M** (2010) Short term variations of tracer transit speed on alpine glaciers. *The Cryosphere* **4**(3), 381–396. doi: [10.5194/tc-4-381-2010](https://doi.org/10.5194/tc-4-381-2010)
- Young TJ and 8 others** (2018) Resolving the internal and basal geometry of ice masses using imaging phase-sensitive radar. *Journal of Glaciology* **64** (246), 649–660. doi: [10.1017/jog.2018.54](https://doi.org/10.1017/jog.2018.54).

Appendix

Table A1. Battery life calculation

Activity	Quantity	Unit
Energy consumption during measure and transmit	0.5	J
Duration of measure and transmit	3.2	s
Current consumption during sleep	500	nA
Nominal battery voltage	3.7	V
Power consumption during sleep	1.85	uW
Battery nominal voltage	3.7	V
Battery nominal capacity	400	mAh
Battery nominal capacity	1.48	Wh
Battery nominal capacity	5328	J
Derate factor for operating in the cold	50%	
Battery effective capacity in the field	2664	J
For 2 measurements per day:		
Active measurement time per day	6.4	seconds
Sleep time per day	86393.6	seconds
Energy used while active	1	J
Energy used while asleep	0.16	J
Total energy used per day	1.16	J
Number of days the system will run for	2296	days
Number of years the system will run for	6.3	years